論文 / 著書情報
Article / Book Information

論題(和文)	
Title(English)	Pressure Oscillation Accompanying Steam Discharge into Subcooled Liquid Pool
著者(和文)	宇多村 元昭
Authors(English)	Motoaki Utamura
出典(和文)	, Vol. 29, No. 258, pp. 4197-4208
Citation(English)	Bulletin of JSME, Vol. 29, No. 258
発行日 / Pub. date	1986

Bulletin of JSME, Vol. 29, No. 258 December 1986

Paper No. 258-33

Pressure Oscillation Accompanying Steam Discharge into Subcooled Liquid Pool*

By Motoaki UTAMURA**

Pressure oscillation may be induced in liquid when steam is injected into subcooled liquid through a submerged pipe. Theoretical and experimental considerations have been made on mechanism of the pressure oscillation in the case that an oscillatory condensation interface exists at the pipe exit. The pressure oscillation is triggered by a physical process in a vapor phase, being strongly affected by the type of condensation heat transfer at the vapor-liquid interface. A heat-transfer mechanism proposed here well explains parametric effects on various characteristics of the pressure oscillation. A new dimensionless parameter of subcooling is proposed which correlatees water and freon data better than Jacob number. Operational ranges for the onset of pressure oscillation as well as its frequency and amplitude are obtained in analytical forms which are verified by experiments in a wide range of parameters.

Key Words : Pressure oscillation, Steam condensation, Condensation heat transfer, Frequency, Amplitude

1. Introduction

Direct vapor condensation in subcooled liquid is a common phenomenon encountered in many two-phase systems. Of specific interest here is vapor injection into subcooled liquid. Most of the research on vapor jet condensation have been experiment-oriented. Several authors (1)-(4) observed various hydro-dynamical behaviors associated with the condensation process. Nariai and Aya(4) qualitatively identified four distinct dynamical regimes, as a function of steam mass flux and water temperature. Dynamic characteristics changes from intermittent condensation at low mass fluxes and low water temperatures to periodic one at intermediate mass fluxes, and to bubbling without high frequency components near the saturation temperature.

At low steam flow rate, the condensation interface becomes unstable, as water comes in and out of the discharge pipe, causing short-duration pressure spikes. This phenomenon, known as "chugging", was examined by several groups (5)-(7).

At intermediate and high steam flow rates, an oscillatory condensation interface forms at the exit of the injection pipe (condensation oscillation). The condensation oscillation produces pressure oscillation inside the discharge pipeline and in the liquid pool, which is the subject of the present study. Its frequency and amplitude vary in a complex manner depending on the liquid subcooling, the rate of steam supply and the geometry and scale of the system (e.g. injection pipe diameter). Fukuda(8) studied some details of the condensation oscillation for both water and freon (R-113) in a wide range of flow rates and temperatures. He revealed that the liquid subcooling played such a dramatic role in condensation process that pressure oscillation was enhanced as the liquid subcooling was lowered down to a certain value but was reduced drastically thereafter in subsonic flow, and that the pressure oscillation was significantly decreased in sonic flow.

Simpson and Chan(9) performed an experiment for water in a temperature range 25-65°C and correlated growth of the oscillation amplitude as a function of Jacob number and Reynolds number. Jones and Dodge(10) have derived a theoretical expression for the amplitude of pressure oscillations. However, these correlation and expression did not explain rapid decrease in the magnitude at near-saturation temperatures.

Several groups(3)(8)-(11) have investigated frequency behaviors with respect to the liquid subcooling, steam velocity and diameter of the injection pipe. As a result, it is generally believed that the frequency of the condensation oscillation increases as the liquid temperature and the pipe diameter decrease, and also as the steam velocity increases. Correlation forms proposed so far, however, were rather diversive, which seems to result mainly from limited data ranges. Hence, assessment still remains to be done using a wide range of experimental parameters.

In short, through extensive past research, phenomenological understanding of the condensation oscillation progressed. However, the mechanism that triggers condensation oscillation and some

* Received 25th January, 1985.
** Research Fellow, Energy Research Laboratory, Hitachi Ltd., 1168 Moriyama-cho, Hitachi, Ibaraki, 316 Japan

of important features of the condensation oscillation remain to be revealed. Therefore, the objective of the present work is to understand the mechanism of condensation oscillation based on a physical model and to demonstrate it by experiments. The frequency, the amplitude and the limit of the condensation oscillation are discussed for both cases of subsonic and sonic flow rates. Specifically, unification of water and freon data was attempted. The parametric effects of liquid subcooling, exit steam velocity and pipe diameter were investigated as well.

Nomenclature

A	= flow area of injection pipe at its exit
a	= exponent of steam velocity in expression of h
b	= geometric constant (Eqs.(12),(15))
C	= sonic velocity of steam ($\equiv \sqrt{(\partial P/\partial \rho)_s}$)
c_p	= specific heat of subcooled liquid at constant pressure
D	= diameter of the injection pipe
d	= diameter of liquid particle entrained from gas-liquid interface
ΔE	= mechanical energy produced within steam jet
F	= function of subcooling and steam velocity defined by (Eq.(17))
f	= frequency of condensation oscillation
G	= steam mass in control volume
h	= condensation heat transfer coefficient on the entrained liquid particles
h_B	= overall condensation heat transfer coefficient in steam jet
J_a	= Jacob number ($\equiv c_p\Delta\theta/L$)
K	= bulk modulus of steam ($\equiv \rho C^2$)
k	= exponent of steam velocity in expression of net heat transfer area
L	= latent heat
ℓ	= exponent of bubble volume in expression of the area of macroscopic vapor-liquid interface
M	= Mach number defined at static system pressure ($\equiv u/C^*$)
m_d	= mass of an entrained liquid particle ($\equiv 4\pi\rho_\ell(d/2)^3/3$)
m_o	= virtual mass attached to interface (Eq.(15))
N	= number of liquid particles entrained per unit area of the interface, per unit time
n	= exponent of steam velocity in expression of overall condensation heat transfer rate ($\equiv a + k$)
p	= pressure
R	= bubble radius
R_e	= Reynolds number
S	= net heat transfer area
S_d	= surface area of an entrained liquid particle
S_I	= surface area of vapor-liquid interface
S_t	= Strouhal number ($\equiv fD/C$)
s	= Laplace parameter
t	= time
t_s	= time constant ($\equiv G_o/W_o$)
u	= steam velocity at the entrance of the control volume
V	= volume of the control volume
W_o	= steam flow rate at steady state
W_{in}	= steam inflow rate into the control volume
W_c	= rate of steam condensation in the control volume
x	= static quality of saturated steam in the control volume
δZ	= infinitesimal variation of physical variable Z
ρ	= density
σ	= surface tension force of subcooled liquid
μg	= viscosity of steam
$\Delta\theta$	= liquid subcooling
θ_{sat}	= saturation temperature
τ_1	= average life time for a subcooled liquid particle to reach saturation ($\equiv c_p m_d/(hS_d)$)
π_c	= dimensionless subcooling ($\equiv \rho L\Delta\theta/(K\theta_{sat})$)
π_c^*	= π_c defined at the entrance of the control volume
$\bar{\pi}_c$	= demensionless critical subcooling as a solution of the equation F = 0
ω	= angular frequency

Subscripts

o	= steady state
e	= entrainment
g	= dry steam
ℓ	= liquid phase
d	= entrained liquid particle
I	= macroscopic vapor-liquid interface
w	= water

Superscripts

o	= steady state
*	= entrance of the control volume
~	= non dimension
^	= representative value

2. Theory

2.1 Model description

Figure 1 shows the concept of the present model. Steam is discharged from an opening into subcooled liquid and is supposed to form a jet with macroscopic vapor-liquid interface. A control volume is set up in the steam jet. Based on the mass balance of steam and the equations of

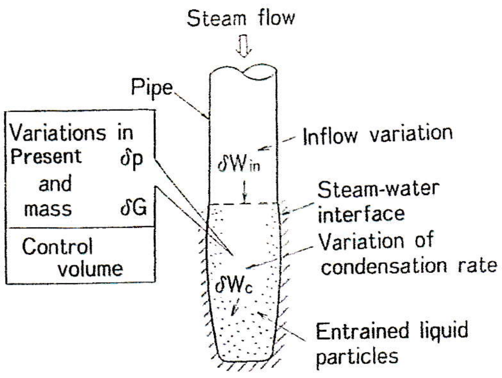

Fig. 1 Concept of model

state and of liquid motion, the system response to the pressure perturbation inside the control volume is analyzed. Basic assumptions made in the analysis are as follows:

(1) Each physical quantity consists of a steady part Z_0 and a time-dependent infinitesimal variation δZ;
(2) steam in the control volume is homogeneous, saturated and in the thermodynamic equilibrium;
(3) the pressure wave propagates upstream into the pipeline and the magnitude of the reflection wave is negligibly smaller than that of the incident wave at the entrance of the control volume;
(4) entrainment is present and steam condensation occurs primarily on the surface of entrained liquid particles;
(5) the condensation heat-transfer coefficient depends on the steam velocity at the entrance of the control volume while it is independent of the pool subcooling;
(6) macroscopic interfacial area is in a geometric relation with the steam volume; and
(7) liquid inertia is represented by a virtual mass attached to the control volume.

The statement of the assumption (3) implies no interaction between steam jet and steam column in the pipeline, which holds if length of the pipeline is infinite. However, even in a high steam velocity region where condensation oscillation is expected to occur, it is valid in a practical range of pipeline lengths, because the higher the velocity, the lower the eigen-frequency of the steam column, which was examined in the experiment[8].

The assumption (4) is based on Wallis' correlation[12] which predicts the gas velocity range sufficient to entrain droplets from horizontal liquid film,

$$\frac{u\mu_g}{\sigma}\left(\frac{\rho_g}{\rho_\ell}\right)^{1/2} \geq 2.46\times10^{-4} \quad \cdots (1)$$

Under the condition of an intermediate liquid temperature in atmosphere, Eq.(1) shows that $u > 30\mathrm{m/s}$ ($\approx 18\mathrm{kg/m^2s}$) which corresponds to the range of condensation oscillation in most experiments [3][4][8]. In the case of steam jet emerged in liquid, the lower limit of the velocity range is expected to be less than in the above situation due to the presence of buoyancy to cause unstable motion of the vapor-liquid interface. Once entrainment is initiated, a number of subcooled liquid particles may be created. Hence, most steam is supposed to condense on the particles. This mechanism may be similar to dropwise condensation whose heat-transfer coefficient is independent of subcooling except the case of very large subcoolings. Therefore, the assumption (5) may be valid.

The assumption (7) is based on the observation that frequency of the condenation oscillation is relatively high[11], which means that liquid flow field is acceleration-dominated. The other assumptions will be verified by comparing the analytical results with experiments.

2.2 Basic equations

Based on the assumptions (1) and (2), variations of thermodynamic quantities $\delta\rho$, $\delta(\Delta\theta)$ and δp are related as follows:

$$\delta\rho = \rho_0\ \delta p\ /\ K \quad \cdots (2)$$

where, subscipt o denotes the steady state.

Noting that $\delta(\Delta\theta) = \delta(\theta_{sat})$, Clapeyron-Clausius relation gives

$$\delta(\Delta\theta) = \theta_{sat}\ \delta p\ /\ (\rho_0 L) \quad \cdots (3)$$

In the case of subsonic flow, incorporating a progressive plane wave relation [13] based on the assumption (3), we can write the variation of steam velocity at the entrance of the control volume as

$$\delta u = -\ \delta p\ /\ (\rho_0{}^*\ C^*) \quad \cdots (4)$$

where, superscript * denotes the entrance of the control volume.

In the case where the flow is choked at the pipe exit, the steam flow way experience isentropic expansion outside the pipe, developing a supersonic flow. Since the velocity of the supersonic expansion flow is influenced by the ambient pressure, the steam velocity in the present case is influenced by the pressure oscillation within the steam jet. Defining the entrance of the control volume in this case at the place where pressure of free jet reaches the static pressure of the pool system, we get an alternative to Eq.(4) as

$$\delta u = -\ \delta p\ /\ (\rho_0{}^* C^* M) \quad \cdots (4)'$$

in the choked flow case, where Bernoulli's equation $d(u^2/2) + dp/\rho_0{}^* = 0$ and Mach number $M(\equiv u_0/C^*)$ are used in deriving Eq.(4)'.

Mass balance of steam in the control volume yields

$$\frac{d\delta G}{dt} = \delta W_{in} - \delta W_c \quad \cdots (5)$$

where,

$$W_{in} = \rho^* A u \quad \cdots (6)$$

$$W_c = hS\Delta\theta/L \quad \cdots (7)$$

The variation of mass inflow rate δW_{in} in the case of subsonic flow at the entrance of the control volume is given by

$$\delta W_{in} = W_{in}{}^{\circ}(\delta\rho^*/\rho_0{}^* + \delta u/u_0),\ M<1 \quad \cdots (8)$$

where $\delta\rho^*$ is expressed as

$$\delta\rho^* = \rho_o^* \delta p / K^* \quad \cdots (9)$$

similarly to Eq.(2).

Note that the mass flow rate is not affected by the pressure condition at the downstream where a choked flow is established at the pipe exit. Then, the variation of mass inflow rate at the entrance of the control volume becomes naught, that is

$$\delta W_{in} = 0, \; M \geq 1 \quad \cdots (8)'$$

The variation of condensation rate in Eq.(5) may be expanded to give

$$\delta W_c = W_c^\circ \, (\delta h / h_o + \delta S / S_o) \quad \cdots (10)$$

Condensation heat transter coefficient appearing in Eqs.(7) and (10) may be written as

$$h = \eta u^a \quad \cdots (11)$$

under the assumption (5). Here, η is a constant independent of variables u and $\Delta\theta$.

Derivation of net heat-transfer area S in Eqs.(7) and (10) is described below. Figure 2 shows a heat-transfer mechanism hypothesized.

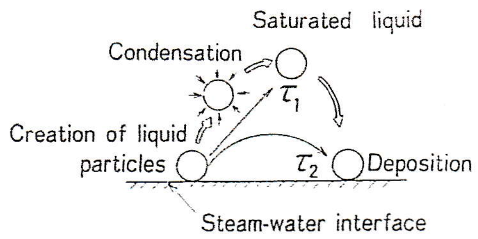

Fig.2 Heat transfer mechanism hypothesized in the model

An entrained subcooled liquid particle absorbs latent heat by steam condensation on its surface, decreases its subcooling and eventually becomes saturated. During or after this process, the liquid particle is deposited on the vapor-liquid interface and disappears from the vapor phase. Hence, two processes exist that deprive a liquid particle of heat trasfer capability, i.e. self saturation (process A) and deposition (process B) with average life times τ_1 and τ_2, respectively. The diameter of the liquid particle may be evaluated by the correlation $\rho_g(u_g - u_\ell)^2 d/\sigma = 10$[14] which is applicable to a liquid film under a sudden acceleration. Let u_g ($\gg u_\ell$) be a typical value of 200m/s, then d = 2.5 10^{-2} mm will be obtained. Consideration of transient heat conduction in the particle with h assumed to be 10^6W/m^{2}K gives 0.02ms for τ_1. Hence, we have $\tau_1 \ll 1/f$ if we take f = 500Hz, the highest frequency observed in the experiment[8]. This means that the process A is virtually a static one relative to the characteristic period of condensation oscillation. Considering the flight distance of the particle during the period τ_1, it is reasonable to assume $\tau_2 \gg \tau_1$. Therefore, the process B is neglected.

Now, we may try to interpret the decrease in the subcooling of the particle effectively by the decrease of the heat-transfer area, with the subcooling kept constant at its initial value, i.e. pool subcooling. Then, the net heat-transfer area in the characteristic time scale in the condensation oscillation is shown to be $S = \tau_1 S_e S_I$ ($S_e \equiv N S_d$), where, τ_1 is a function of the diameter of liquid particle d. d and Se are primarily functions of u in the entrainment theory[14]. Thus, $\tau_1 S_e$ is supposed to be a function of u. As for S_I, from the assumption (6), the following relation is assumed.

$$S_I = b_I V^\ell \quad \cdots (12)$$

The exponent "ℓ" assumes geometrical similarity of jet shape on scaling. The value of "ℓ" must become two thirds provided the similarity of the jet configuration is preserved on scaling geometry (e.g. scaling pipe diameter) with the operational parameters $\Delta\theta$ and u kept unchanged. In the case that the jet shape is spherical, we have $b_I = (4\pi)^{1/3}\, 3^{2/3} = 4.836$. Consequently, net heat-transfer area S becomes

$$S = \xi u^k V^\ell \quad \cdots (13)$$

where, ξ is a constant independent of variables u, V and $\Delta\theta$.

Noting the relation $G = \rho V$, we have its variational form as

$$\delta G / G_o = \delta\rho/\rho_o + \delta V / V_o \quad \cdots (14)$$

The bulk pool motion was modeled in a simplified manner based on the assumption (7). Formal generalization of Reyleigh equation for a spherical bubble was made in terms of jet volume V from the relation $V = 4\pi R^3/3$, giving

$$\left.\begin{aligned} \delta p &= m_o \frac{d^2 \delta V}{d\, t^2} \\ m_o &= b_\ell \rho_\ell V_o^{-1/3} \end{aligned}\right\} \quad \cdots (15)$$

in which higher order variations (e.g. $(\delta V)^2$ etc.) were neglected. Here, b_ℓ is a dimensionless parameter to characterize the jet configuration. In the case of a sphere, b_ℓ is $(4\pi)^{-2/3} 3^{-1/3} \simeq 0.128$ and Eq.(14) reduces to Rayleigh equation without a non-linear term.

In summary, the basic equation system consists of eleven equations (Eqs.(2) $\sim$ (5), Eqs.(8) $\sim$ (11), Eqs.(13) $\sim$ (15)) and variable vector δX having the same number of components $X^T = (p, \rho, \Delta\theta, u, G, W_{in}, \rho^*, W_c, h, S, V)$.

2.3 Condition for condensation oscillation onset

2.3.1 Subsonic flow

By use of the basic equation set except Eq.(15) that exhibits liquid inertia, the following relation between δG and δp was derived

$$t_s \frac{d\delta G}{dt} + \ell \delta G \doteqdot \frac{G_o}{K} F \delta p \quad \cdots (16)$$

where

$$F = \varepsilon + \ell - \{\varepsilon(1-a-k)C^*/u_o\} - K\theta_{sat}/\rho_o L \Delta\theta_o \quad \cdots (17)$$

and

$$\varepsilon = K/K^* \quad \cdots (18)$$

In deriving Eqs.(16)$\sim$(18), relations for the steady state $W_{in}{}^o = W_c{}^o \equiv W_o$, $ts = G_o/W_o = \rho_o V_o/\rho_o{}^* A u_o$ which means time required to consume steam in the control volume by condensation, and a relation for the bulk modulus $K^* = \rho_o{}^* C^{*2}$ were used.

Now, assuming the pressure variation to be a harmonic oscillation with a small amplitude $|\delta p|$ and an angular frequency ω, we can deduce the mechanical energy produced within the control volume from Eq.(16) as

$$\Delta E = \oint \delta p \frac{d\delta V}{dt} dt = \frac{V_o}{G_o} \int_0^{\frac{2\pi}{\omega}} \delta p \frac{d\delta G}{dt} dt \quad \cdots (19)$$

$$= \pi K V_o \omega t_s F |\delta \tilde{p}|^2 / (\ell^2 + \omega^2 t_s{}^2)$$

where, $\delta\tilde{p}$ is a dimensionless group of pressures defined by $\delta\tilde{p} = \delta p/K$.

Hence, the condition for the system to create a positive mechanical energy, $\Delta E > 0$, is equivalent to $F > 0$, that is

$$F = \varepsilon(1-1/M) + (\ell + \varepsilon n/M) - 1/\pi_c > 0 \quad \cdots (20)$$

where, $n = a + k$ and

$$\pi_c = \rho_o L \Delta\theta_o / (K\theta_{sat}) \quad \cdots (21)$$

A dimensionless group π_c provides a measure of the subcooling under a variable ambient pressure with a constant liquid temperature, since the relation $\delta(\pi_c) = \delta\tilde{p}$ holds from Eq.(3) and Eq.(21).

A physical meaning of each term appearing in Eq.(20) follows. The first term comes from the inflow variation δW_{in}, the second and the third from the condensation variation δW_c. To be more specific, the second term is due to the variation of a product of the net heat-transfer area and the heat-transfer coefficient, i.e. $\delta(hS)$ and the third term due to the variation of subcooling. The second term is seen to excite the system and the others to suppress the system excitation. Figure 3 shows responses of quantities to the pressure perturbation. The mechanical energy is produced when F is positive (Eq.(19)). Under this condition, mass variation follows pressure variation, causing condensation oscillation as shown in Fig.4.

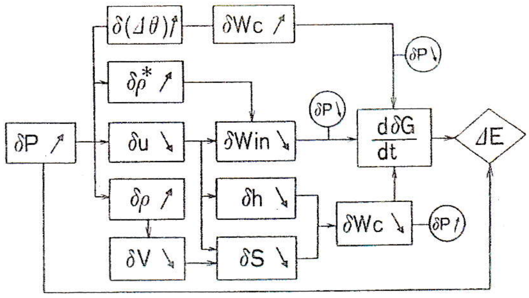

Fig.3 Mechanism of condensation oscillation

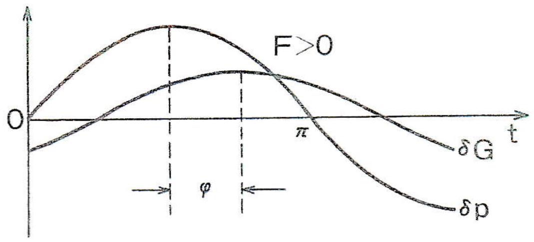

Fig.4 Phase relation between variations of pressure and vapor mass

Equation (20) can be simplified. From following relations and an approximation, $1/\rho_o = x/\rho_g + (1-x)\rho_\ell$, $C^2 = xC_g{}^2$ (good approximation in the range $x > 0.1$) and $\rho_g/\rho_\ell = 0$, we can reduce $\rho_o = \rho_g/x$, $K = K_g \equiv \rho_g C_g{}^2$ and then $\varepsilon = 1$. Thus, Eq.(20) can be rewritten as

$$F = 1 + \ell - (1-n)/M - x/\pi_c{}^*, \quad M < 1 \quad \cdots (22)$$

where

$$\pi_c{}^* = L\Delta\theta_o/(C_g{}^2\theta_{sat})$$

2.3.2 Choked flow at pipe exit

Following the procedure in 2.3.1 using Eqs.(4)' and (8)' instead of Eqs.(4) and (8), the same form of mechanical energy formulation as Eq.(19) can be obtained provided the function F is replaced by

$$F = \ell + n/M^2 - x/\pi_c{}^*, \quad M \geqq 1 \quad \cdots (22)'$$

The above results of Eqs.(22), (22)' were obtained excluding the liquid inertia equation (Eq.(15)). Alternatively, based on the whole set of basic equations, application of Routh-Hurwitz instability criterion to the system characteristic equation was found to yield the same results as above. This suggests that key mechanism to create condensation oscillation is related to thermodynamics of vapor phase.

2.3.3 Regime map of condensation oscillation

Figure 5 shows the ranges that satisfy inequalities given by Eqs.(22) and (22)'.

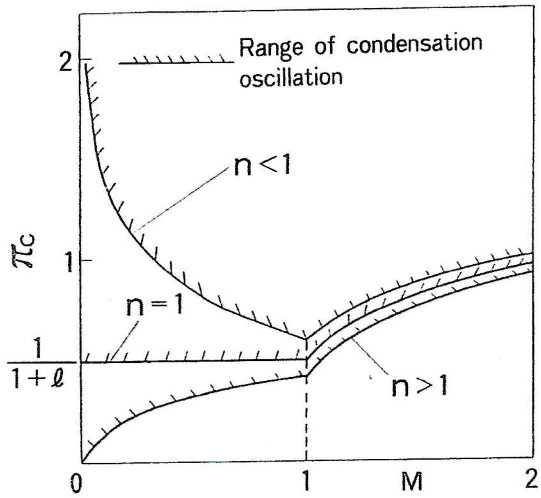

Fig.5 Range of condensation oscillations

In the figure, π_c corresponds to $\pi_c{}^*/x$. Possibly, three kinds of regimes may exist depending on the value of parameter "n". Recalling the definition of "n", it represents an exponent of steam velocity in the expression of condensation rate. Referring to the past works(8)(10), "n" must be positive and less than unity. Fukuda(8) proposed from his experiment that the overall heat-transfer coefficient based on the macroscopic interface area be proportional to $Re^{0.9}$, which is the only correlation available. Therefore, we assume that n = 0.9 in the following discussions. The subcooling at the boundary where the condensation oscillation terminates is shown to decrease with steam velocity in the subsonic flow region, while it increases in supersonic flow region. This tendency agrees with experimental observations in the past(2)(8).

2.4 Frequency analysis

Based on the basic equations, the system characteristic equation becomes

$$m t_s s^3 + m(\ell - F) s^2 + t_s s + \ell = 0 \qquad \cdots (23)$$

where s is the Laplace parameter and $m = m_o V_o / K$. Equation (23) may be approximated by

$$m t_s s^3 + \ell = 0 \qquad \cdots (24)$$

if we note that principal terms to characterize eigen frequency are the first, the third and the fourth terms in Eq.(23), and that $\ell \gg t_s\,\omega$ from experimental data on frequency. Imaginary part of the solution of Eq.(24) yields

$$\left.\begin{aligned} \omega &= \frac{\sqrt{3}}{2}\left(\frac{\ell}{m t_s}\right)^{1/3} = \zeta_1 R_0{}^{-5/3} M^{1/3} D^{2/3} \\ \zeta_1 &= \frac{\sqrt{3}}{2}\left(\frac{3}{4\pi}\right)^{5/9}\left(\frac{\pi \rho_o{}^* C^* K \ell}{4 \rho_o \rho_\ell b_\ell}\right)^{1/3} \end{aligned}\right\} \cdots (25)$$

in which the equivalent radius of the jet R_o can be derived from the steady relations to give

$$\left.\begin{aligned} R_0 &= \hat{R}\pi_c{}^{-1/3\ell} M^{(1-n)/3\ell} \\ \hat{R} &= \zeta_2 D^{2/3\ell} \\ \zeta_2 &= \left(\frac{3}{4\pi}\right)^{1/3}\left(\frac{\pi \rho_o \rho_o{}^* L^2 C^{1-n}}{4\xi n K\ \theta_{sat}}\right)^{1/3\ell} \end{aligned}\right\} \cdots (26)$$

Incorporating these relations, we have an expression for frequency f ($\equiv \omega/2\pi$) as

$$\left.\begin{aligned} f &= \zeta_3\ \pi_c{}^{\alpha}\ M^{\beta}\ D^{\gamma} \\ \zeta_3 &= \zeta_1\ \zeta_2{}^{-5/3}/2\pi \end{aligned}\right\} \cdots (27)$$

where $\alpha = 5/9\ell$, $\beta = -\alpha(1-n) + 1/3$, $\gamma = -2(\alpha - 1/3)$ and ζ_3 is a constant with a velocity dimension. The parameter "ℓ" and the constant ζ_3 are to be determined by experimentation. However, with the assumption that the jet shape keeps a geometric similarity (i.e. $\ell = 2/3$), we can obtain non-dimensional expressions for bubble radius $\tilde{R}_o$(= R_o/D) and frequency S_t(= fD/C) with dimensionless constants $\tilde{\zeta}_2 = \zeta_2(\ell = 2/3)$ and $\tilde{\zeta}_4 = \zeta_3/C$ as follows

$$\left.\begin{aligned} \tilde{R}_o &= \tilde{\zeta}_2\ \pi_c{}^{-0.5} M^{0.05} \\ S_t &= \tilde{\zeta}_4\ \pi_c{}^{5/6} M^{1/4} \end{aligned}\right\} \cdots (27)'$$

Table 1 compares the functional form of Eq.(27)' with those appearing in the past literature.

Table 1 Frequency correlations

$$f \propto \Delta\theta^{\alpha} u^{\beta} D^{\gamma}$$

	Exponent	α	β	γ
*	Jones & Dodge	$\frac{3}{4}$	0.068	-1
	Aya, Nariai & Wakabayashi	$\frac{2}{3}$	0.3	$-1 \sim -\frac{2}{3}$
	Present	$\frac{5}{6}$	$\frac{1}{4}$	-1
**	Aya, Nariai & Wakabayashi	0.68	0	$-\frac{2}{3}$
	Fukuda	1	0	-1
	Arinobu	1.4	1	-1
	Simpson & Chan	0.72	1.25	-0.75
	Sursock & Duffey	1	0	0

* Theoretical or Semi-empirical

** Purely empirical

2.5 Analysis of mechanical energy

Using the assumption $\ell^2 \gg \omega^2 t_s^2$ made in section 2.4, we can simplify Eq.(19) to obtain

$$\Delta E = \pi K V_0 \omega t_s F |\delta\tilde{p}|^2/\ell^2 \qquad \cdot\cdot\ (28)$$

Product $V_0 \omega t_s' F$ is a function of M and π_c. Defining $\bar{\pi}_c$ as a function of M that satisfies F = 0 (Eq.(22) or (22)'), and incorporating Eqs.(25) and (26), we can expand Eq.(28) to get

$$\Delta e = (\pi_c/\bar{\pi}_c - 1)\pi_c^{-(\delta+1)} M^{\delta(1-n)-2/3} \qquad \cdot\cdot\ (29)$$

where, $\delta = 13/9\ell$ and Δe is a dimensionless mechanical energy defined by $\Delta E/(K\hat{V}_0|\delta\tilde{p}|^2)$ in which $\hat{V}_0$ is a representative jet volume proportional to $A\delta^{-2/3}$. Obviously, Δe becomes zero at $\pi_c = \bar{\pi}_c$, and with M provided, can be shown to have a peak value Δe^{max} at the following subcooling

$$\pi_c^{max} = (1 + 1/\delta)\bar{\pi}_c \qquad \cdot\cdot\ (30)$$

where

$$\bar{\pi}_c = \begin{cases} M/\{(1+\ell)M+n-1\}, & M < 1 \\ M^2/(\ell M^2+n), & M \leq 1 \end{cases} \qquad \cdot\cdot\ (31)$$

3. Experiment

3.1 Apparatus

The test apparatus consisted of a steam generator, a pipeline, an injection pipe and a water tank open to atmosphere as shown in Fig. 6. The injection pipe, having an oepn end, was vertically submerged and located at the center of the water tank. The pipeline was 20m long including the injection pipe and 130.8mm

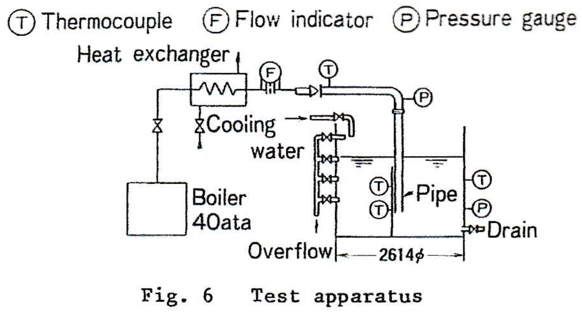

Fig. 6 Test apparatus

in diameter. Saturated dry steam was obtained at the exit of the injection pipe by use of a heat exchanger. The apparatus was operated so that steam was supplied at a constant flow rate. Condensation increased water temperature until near saturation and the water level was controlled to remain unchanged using an overflow line. The dynamic pressure was measured on the tank wall at the same height as the exit of the injection pipe. An instrumentation zig equipped with several thermocouples was installed vertically at a radial distance of 300mm away from the center of the tank. Water temperature distribution was virtually negligible due to good mixing of liquid by the vapor momentum. Experimental parameters were the diameter of the injection pipe (67.9-130.8mmϕ), the pipe submergence (900-1500mm), the steam mass flux (20-270kg/m^{2}S) and the bulk water temperature (20-97.5^{o}C). Feature of this experiment lay in the range of diameters of the injection pipe which was wider than in the past experiments. Effect of the submergence was negligibly small.

3.2 Experimental results

Figure 7 shows pressure-time histories measured at tank wall. The steam mass flux was 82kg/m^{2}S, the diameter of the injection pipe, 130.8mmϕ and the submergence, 900mm.

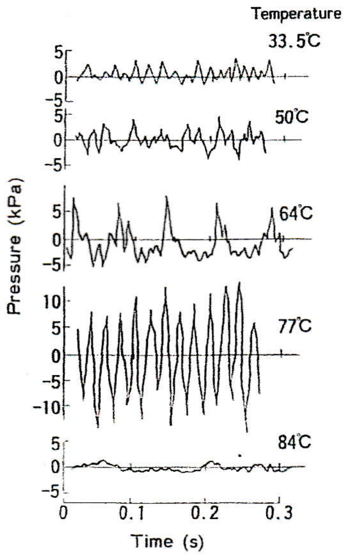

Fig.7 Pressure time histories at tank wall

The pressure amplitudes are seen to grow with the pool bulk temperature to a certain value but show rapid decrease thereafter. The frequency at temperature 77^{o}C shows some resonant behavior. Except this, frequencies show a gradual decrease in general with temperature.

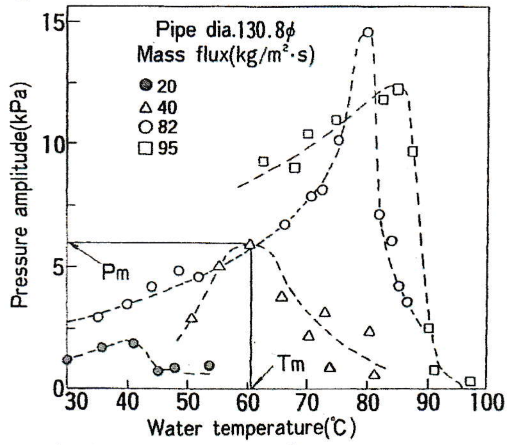

Fig.8 Pressure amplitude and water temperature

The relation between the r.m.s pressure amplitude and the water temperature is shown in Fig.8 with the steam mass flux as a parameter. In each case, there is a temperature (limiting temperature) where the pressure amplitude becomes maximum. This temperature shifts higher with an increasing mass flux. At high steam flow rates, an amplitude drop is distinct where the condensation oscillation tends to cease.

Combinations of the parameters, steam mass flux and water temperature, which give the maximum amplitude Pm are plotted in Fig.9.

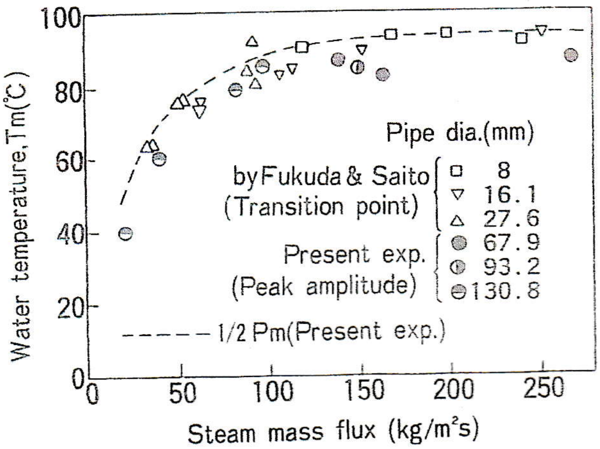

Fig.9 Combinations of steam mass flux and water temperature to cause peak pressures

The data obtained by Fukuda and Saito[15] from smaller scale experiment are also plotted. Their data points are defined as ones giving transition of condensation type. This definition, however, is seen to be equivalent to the condition of giving half the maximum amplitude ($P_m/2$) since the broken line estimated based on the present experiment fits these data. Considering this equivalence, the data by both authors show no essential difference, which indicates that the condition to produce a peak amplitude and most probably the limit of the condensation oscillaiton is not influenced by the scale of the injection pipe within the range of the pipe diameters covered. Further, data tend asymptotically to a certain temperature in a higher steam mass flux region.

4. Comparison between experiment and theory

4.1 Theoretical analysis

Equation (27)' was evaluated assuming a spherical shape of jet. With constants $\rho_o = \rho_o^* = 0.598\text{kg/m}^3$, $L = 2.25\text{MJ/kg}$, $C = C^* = 439\text{m/s}$, $\theta_{sat} = 373.2\text{K}$ and a representative velocity $\hat{u}_o = C/2$, dimensionless constants $\tilde{\xi}_2$ and $\tilde{\zeta}_4$ were evaluated. In doing this, in terms of the overall condensation heat-transfer coefficient h_B, the product "$\xi\eta$" in $\tilde{\xi}_2$ was substituted by $b_T h_B/\hat{u}_o^n$. Figures 10-A and 10-B compare

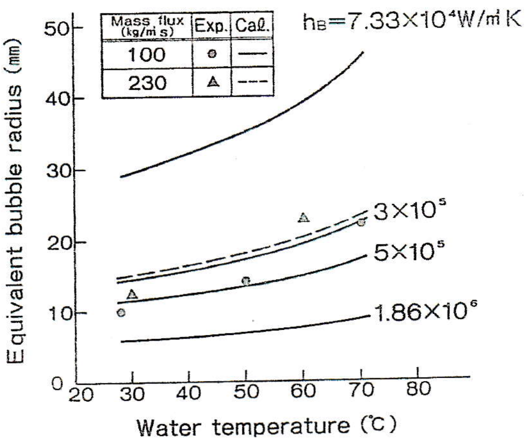

Fig.10-A Equivalent bubble radius

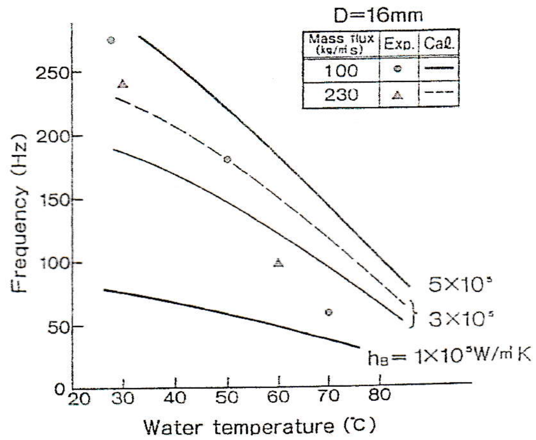

Fig.10-B Frequency of pressure oscillations

calculation results with experiments[8] on the equivalent bubble radius and the frequency, respectively, as a function of the pool water temperature, taking h_B as a calculational parameter. On the other hand, Bankoff's observations covered 7.33×10^4–$1.86\times10^6\text{W/m}^2\text{K}$ for h_B in turbulent subcooled liquid stream[16]. Taking this into consideration, calculations show good agreement with data in a physically justifiable parameter range.

In order to complete theoretical expressions (Eq.(27)'), dimensionless proportional constant $\tilde{\zeta}_4$ was determined. One hundred and twenty four points of frequency data from the present and other experiments[8][17] were incorporated. These covered a wide range of parameters, i.e. $8 \lesssim D \lesssim 130.8$mm in the pipe diameter, $63 \lesssim w \lesssim 269\text{kg/m}^2\text{s}$ in the steam mass flux, $2.8 \lesssim \Delta\theta_o \lesssim 92.6$K in the bulk water subcooling and $11 \lesssim f \lesssim 624$Hz in the frequency. The analysis gave 5.558×10^{-3} for $\tilde{\zeta}_4$ which was equivalent to $3.78\times10^5\text{W/m}^2\text{K}$ of the value of h_B. As a result, we have

$$S_t = 5.558\times10^{-3}\pi_c^{*5/6} M^{1/4} \quad \cdots (27)''$$

Figure 11 compares the frequency predicted by Eq.(27)'' with the measured one, which shows good agreement.

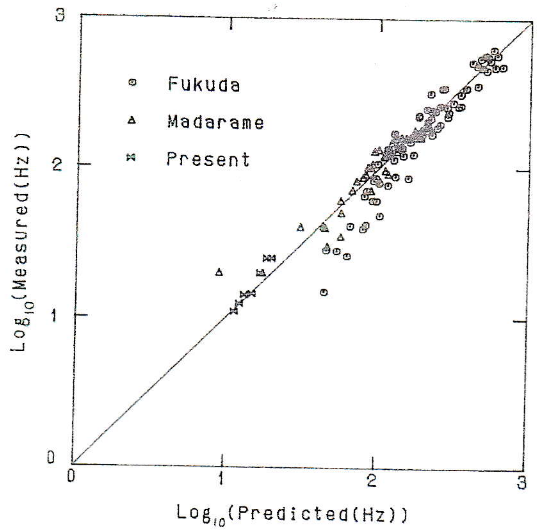

Fig.11 Accuracy of theoretical correlation on frequency (Eq.(27)")

4.2 Regression analysis on frequency and determination of parameter "ℓ".

Next, a multivariate regression analysis was carried out to determine geometric similarity parameter "ℓ" and constant ζ_3 appearing in Eq.(27). Parameter "n" was fixed at 0.9 as was explained in section 2.3.3. The regression gave ℓ = 0.684 and ζ_3 = 2193 with D taken in millimeters. The resultant correlation became

$$f = 2193\ \pi_c^{*0.812} M^{0.252} D^{-0.958} \quad \cdots (32)$$

Figures 12-A and 12-B compare the present semi-empirical correlation (Eq.(32)) with other author's[11] using the same frequency data as in Fig.11.

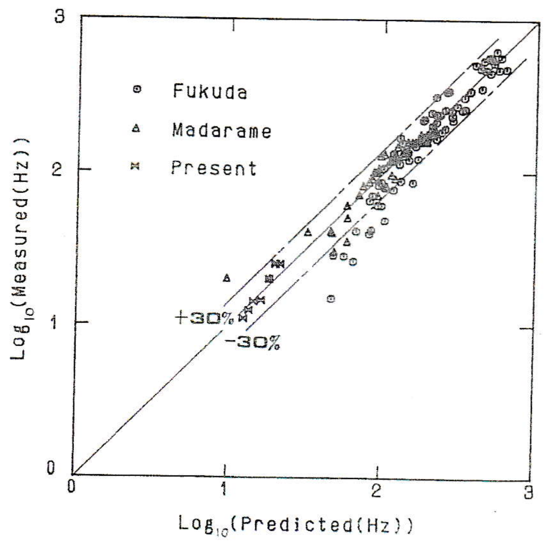

Fig.12-A Accuracy of semi-empirical correlation (Eq.(32))

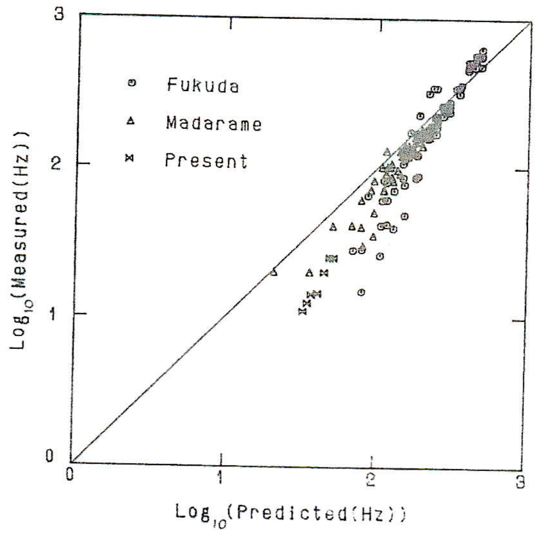

Fig.12-B Prediction by empirical correlation (by Aya et al.[11])

It is seen that Eq.(32) produced 30% prediction error and accuracy was much improved. The value ℓ = 0.684 gives $S_I \propto V_o^{0.684}$ in Eq.(12), which suggests that similarity of jet configuration is almost preserved on scaling pipe diameter because "ℓ" value is quite close to the theoretical value of 2/3 (= 0.667) in which case geometric similarity is exactly maintained. This observation was confirmed by the fact that both predictions by Eqs.(27)" and (32) were very close to each other from comparison of Figs. 11 and 12-A.

4.3 Amplitude

The mechanical energy produced in the steam jet is transformed into the kinetic energy of surrounding liquid which eventually produces a dynamic pressure in liquid. Thus, the mechanical energy may be related to the magnitude of pressure oscillation induced in water. Noting the relation that mechanical energy is proportional to the square of dimensionless amplitude $|\delta\tilde{p}|$ in vapor phase shown in Eq.(28), we try to correlate the amplitude of the pressure oscillation using the square root of the dimensionless mechanical energy (Eq.(29)). Using the result of the frequency analysis ℓ = 0.684, an undetermined parameter "δ" becomes 2.112 and the resultant correlation for the dimensionless amplitude considering the spatial attenuation effect yields

$$\Delta P/\kappa P_o = \lambda (D/2r)(\pi_c^*/\bar{\pi}_c^* - 1)^{1/2} \times \pi_c^{*-1.56} M^{-0.228} \quad \cdots\cdots (33)$$

where, λ and κ denote a dimensionless constant and a polytropic index for dry steam, respectively. π_c and $\bar{\pi}_c$ in Eq.(29) were replaced by π_c^* and $\bar{\pi}_c^*$ respectively in order to enable the correlation to be compared with experiment. π_c^* can be derived by rearranging Eq.(31) with the relation $\pi_c = \pi_c^*/x$ in which steam quality "x" was chosen to be 0.428 which was determined by the analysis described later in section 4.4. Taking λ as 0.76, Fig.13 compares calculation by Eq.(33) with experiment.

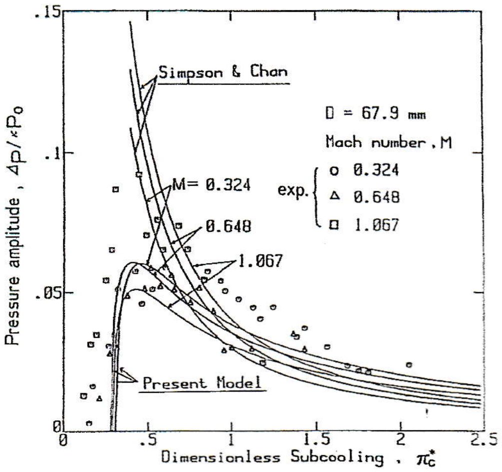

Fig.13 Predicted amplitude in comparison with experiment

The trend of amplitude with subcooling has been shown to be well predictable. Calculation was also made using Simpson & Chan's correlation(9) which had been confirmed in the range of pool temperatures 25°C-75°C equivalent to the range 1.1-2.35 in terms of π_c^*. Both results agreed well in an intermediate subcooling.

The reason why pressure amplitude has a peak with respect to subcooling can be explained as shown in Fig.14. The mechanical energy is proportional to $V_o t_s \omega F$ in which $V_o t_s$ has a positive gradient and ωF negative with subcooling decreased if we recall Eqs.(20),(26) and (27).

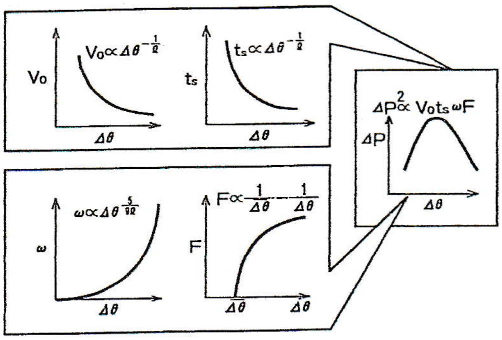

Fig.14 Water subcooling effect on pressure amplitude

The former is dominant at high subcooling and the latter is dominant at low subcooling, which results in a peak amplitude at an intermediate subcooling. Physical interpretation follows. As the subcooling is decreased, the rate of condensation comes to be decreased, which causes growth of bubble volume V_o and thus steam consumption time t_s to be longer. These two cause a larger volume change in a bubble when unit pressure change is applied, which induces a larger dynamic pressure in the liquid pool. On the other hand, as the subcooling is decreased, the bubble frequency is reduced, which gives a slower bubble motion to cause a smaller dynamic pressure in the liquid pool. The variation of steam temperature due to unit pressure change influences the change in the rate of steam condensation. This effect, shown in F, is dominant at a low subcooling and reduces mechanical energy drastically as the subcooling is decreased.

Figure 15 depicts trend of the peak amplitude with steam velocity.

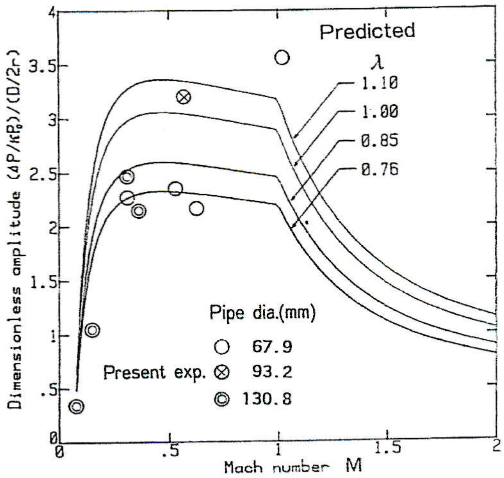

Fig.15 Peak amplitude dependence on Mach number

Calculation shows a rapid increase in the amplitude up to the Mach number 0.4 and then a gradual decrease until a choked flow is established. In supersonic flow, the amplitude decays significantly as the steam velocity increases. In the range of experimentation, experiment and calculation are shown to agree well. In experimental observations the condensation in a choked flow was not so noisy as in a subsonic flow(8)(9), which verifies the trend of the present analysis qualitatively.

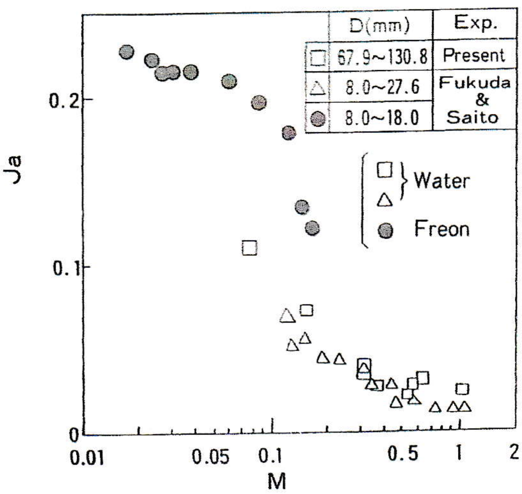

Fig.16 Threshold of condensation oscillation in terms of Jacob number

4.4 Condensation oscillation limit

Figure 16 is a dimensionless expression of data given in Fig.9 together with freon (R-113) data obtained by Fukuda et al.[15]. The water temperature and the steam mass flux were replaced by the Jacob number ($\equiv c_p\Delta\theta_o/L$) and the Mach number ($\equiv u_o/C^*$), respectively. The freon data are about twice as large as water data at the same steam velocity. Hence, it was not proper choice to use the Jacob number as a dimensionless subcooling. Nor was the use of density weighted with the Jacob number.

An alternative approach was attempted with a new dimensionless subcooling π_c^* ($\equiv L\Delta\theta_o/(C_g{}^2\theta_{sat})$) instead of the Jacob number as shown in Fig.17. Obviously, a much better unification of both data has been achieved except a part of freon data in the range of $M < 0.075$ where no water data were present. It was observed that these freon data belonged to a condensation type, in which liquid reentry into injection pipe occurred on a small scale[15], unlike the condensation oscillation. Hence, as for condensation oscillation, a regime map among different materials can be defined by π_c^* better than by the Jacob number.

Analyses were conducted to predict conditions to limit condensation

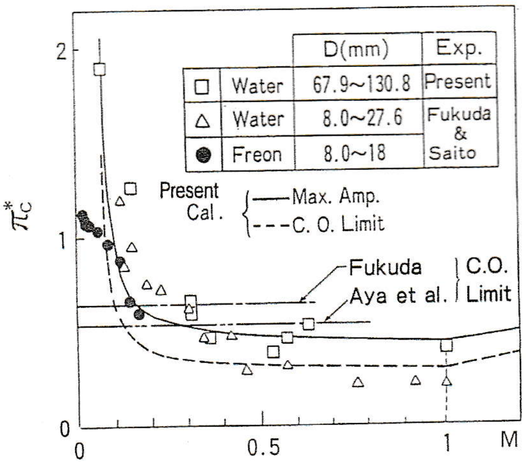

Fig.17 Threshold of condensation oscillation in terms of π_c* and predictions

oscillation and to give rise to peak amplitude of condensation oscillation. The broken line in Fig.17 shows condensation oscillation limit (Eqs.(22) and (22)') and the solid line shows the condition where peak pressure appears (Eqs.(30) and (31)). Thus, area between above mentioned two curves covers transition region. In Eqs.(30) and (31), $\pi_c{}^{max}$ was replaced by π_c^*/x. A set of parameter values for "ℓ" and "n" were 0.684 and 0.9 respectively which are the same as used in frequency analysis and the remaining parameter "x", static quality of saturated steam in the control volume, was determined as x = 0.428 so that the solid line fit the data of the present experiment. The value of "x" thus determined was found to be in a physically justifiable range, because an entrainment experiment using a co-current ascending tube had shown that static quality was around 0.6 in the range of gas-phase mass fluxes $50 < w < 80 kg/m^2s$[14].

Correlations for limiting subcooling by other authors[8][18] are also shown, both of which failed to predict the steam velocity effect. On the contrary, the present analysis represented the velocity effect and accomplished a qualitative agreement in the range of steam velocity $0.3 < M < 1$. Calculation, however, tends to underestimate data below that velocity range. Most probably, the reason may be in (1) the rate of entrainment and (2) the thermodynamic non-equilibrium effect at a low steam velocity. At a lower steam velocity, the rate of entrainment might be decreased, resulting in a higher static quality.

The second reason is that the lower the steam velocity, the higher the frequency along the calculation curve, because the corresponding subcooling is increased. Generally, the phase change can not follow a rapid transient to show the quasi-isentropic process which causes the apparent steam velocity to be higher than in the thermodynamic equilibrium process, i.e. $C^2 > xCg^2$. This effect is equivalent to a higher static quality in the present analysis. This hypothesis may be verified by Mori et al.'s calculation[19] for a two-phase dispersed flow, which shows that $C^2/Cg^2 > 0.9$ for static quality of 0.77 with droplet diameter of 0.1mm. This droplet size is anticipated to be realized in entrainment by the steam velocity of 100m/s ($M = 0.22$) from correlation $\rho_g(u_g - u_\ell)^2 d/\sigma = 10$[14]. Consideration of the above mentioned two mechanisms may result in shifting the calculation result upward at low steam velocity and improve agreement between analysis and experiment in a lower steam mass flux region.

5. Conclusions

The mechanism of condensation oscillation was studied theoretically and experimentally, and some of important characteristics in condensation oscillation have been revealed. Primary conclusions to be drawn follow:

(1) Condensation oscillation is realized under the condition that variation of steam mass in the jet follows the pressure change, which is triggered purely by gas-phase thermodynamics.

(2) A new dimensionless subcooling π_c is proposed which enables regime map of condensation oscillation to be unified between water and freon (R-113).

(3) Limit of condensation oscillation is obtained as a function of dimensionless subcooling π_c^* and Mach number, and it shows no dependence on scaling which has been confirmed by the experiment in the range of pipe diameters $8 \leq D \leq 130.8$mm.

(4) Theoretical and semi-empirical

correlations for frequency of condensation oscillation are obtained, the latter of which fit experiments with precision of 30% for a wide frequency range.
(5) Amplitude dependence on subcooling and steam velocity is clarified and physical explanation is made for the reason why the amplitude has a peak at a certain subcooling.
(6) Characteristics of condensation oscillation depend on two important parameters, a geometric similarity parameter "ℓ" and an exponent "n" of steam velocity in the expression of the rate of condensation. Analysis of the "ℓ" reveals that jet configuration almost preserves geometric similarity on scaling pipe diameter with operational variables, subcooling and steam velocity, kept unchanged.

Acknowledgment

The author would like to express his gratitude to Mr. I. Yokoyama, a technician of Energy Research Laboratory Hitachi Ltd., for his active cooperation in conducting the experiments. He is also indebted to Dr. H. Ogasawara, manager of Hitachi Works, Hitachi Ltd., for his valuable comments.

References

1. Chan, C. K., 6th International Heat Transfer Conference Vol. 5 (1978), pp. 395-400.
2. Cumo, M., Farello, G. E. and Ferrari, G., ibid, pp.101-106.
3. Arinobu, M., Proc. of the ANS/ASME/NRC Int. Topical Meeting on Nuclear Reactor Thermal-Hydraulics Vol. 1 (1980-10), p.293.
4. Nariai, H. and Aya, I., Proc. of ANS/ASME/AIChE 2nd Int. Topical Meeting on Nuclear Reactor Thermal-Hydraulics Vol. II (1983-1).
5. Kowalchuk, W. and Sonin, A. A., U. S. NRC. NURED/CR-0221, (1978-6).
6. Marks, J. S. and Andeen G. B., ASME Condensation Heat Transfer, 18th National Heat Transfer Conference (1979), pp.93-102.
7. Sursock, J. P. and Duffey, R. B., Topics in Two-Phase Heat Transfer and Flow, ASME Winter Annual Meeting (1978).
8. Fukuda, S., Journal of the Atomic Energy Society of Japan (in Japanese), Vol. 24, No.6 (1982-6) pp.64-72.
9. Simpson, M. E. and Chan, C. K., Jouranl of Heat Transfer Vol. 104/271 (1982-5).
10. Jones, D. D. and Dodge, F. T., Trans. ASME, 83-FE-27.
11. Aya, S. and Nariai, H., Reprint of 20th National Heat Transfer Symposium of Japan B315 (in Japanese) (1983-6), pp.283-285.
12. Wallis, G. B., et al., Int. J. Heat and Mass Transfer Vol. 11 (1965-5).
13. Landau, L. D. and Lifshitz, E. M., "Fluid Mechanics," Tokyo Book Company.
14. Akagawa, K., "Gas-Liquid Two Phase Flow," Corona Publishers Company, (in Japanese) (1974).
15. Fukuda, S. and Saito, S., Journal of the Atomic Energy Society of Japan (in Japanese) Vol. 24, No.5 (1982-5).
16. Bankoff, S. G., and Manson, J. P., AIChE Journal, Vol. 8, No.1 (1962-3), pp.30-33.
17. Madarame, H., Proc. of 15th National Heat Transfer Symposium of Japan C206 (in Japanese) (1978-5).
18. Aya, I., et al., Reprint of 16th National Heat Transfer Symposium of Japan A207 (in Japanese), (1979-5), pp.76-78.
19. Mori, Y., et al., Trans. JSME Vol. 37, No.295 (in Japanese) (1971).